Hindawi
Wireless Communications and Mobile Computing
Volume 2022, Article ID 9518542, 15 pages
https://doi.org/10.1155/2022/9518542

Research Article

Multi-Subband Radar Signal Fusion Processing Based on Deep Neural Network in Low Signal-to-Noise Ratio

Yilin Jiang,[1] Sanqiang Tang,[1] Manjun Lu,[2] and Liting Zhang[1]

[1]*Key Laboratory of Advanced Marine Communication and Information Technology, Ministry of Industry and Information Technology, Harbin Engineering University, Harbin 150001, China*
[2]*Shanghai Institute of Radio Equipment, Shanghai 200000, China*

Correspondence should be addressed to Manjun Lu; lmjandy@126.com

Received 28 January 2022; Revised 17 August 2022; Accepted 2 September 2022; Published 28 September 2022

Academic Editor: Abdul Basit

The traditional multi-subband radar signal fusion method based on pole information fits nonlinear signals via linear models. It is very important to accurately estimate the order of the pole model, as the wrong order will lead to errors in the resulting fusion signal. In the case of low signal-to-noise ratio (SNR), it is difficult to obtain accurate pole values. When a noise suppression method is included in the algorithm, the influence of noise on the pole order may be effectively avoided. However, traditional methods have many complex links, and only a few samples can be tested each time. Also, approximating a linear model onto a nonlinear signal will inevitably have errors. Therefore, this paper proposes a method based on the deep neural network (DNN) that applies nonlinear fitting of deep learning to complete the fusion process. The multi-subband distance envelopes are input into the DNN, and the fusion full-band distance envelopes are obtained as the output. Using DNN for subband fusion could improve the radar range resolution and obtain high-resolution one-dimensional range profiles.

1. Introduction

The essence of multi-subband fusion is to extrapolate and predict the vacant frequency band between the high and low subbands. Traditional multiband fusion methods can be divided into two categories. The first category is of nonparametric methods that do not require prior information about the target. Larsson et al. proposed the magnification gap data amplitude and phase estimation method [1] that uses the least squares method to iteratively estimate the unknown spectrum. Simulation and measured data confirm the effectiveness of the method, yet improper initialization may cause the method to fall into a local optimum. Tian et al. modeled the phase deviation of different radars as linear and constant phases [2] using all-phase fast Fourier transform (apFFT) to perform correlation processing on pulse compressed images. However, pulse compression using apFFT loses the initial phase information of the signal and can only display within a small angle range. Upon large angular phase difference, the crossrange window phenomenon occurs, causing estimation errors.

The second category is of parametric methods that establish a parameterized model and solve related parameters. Compared with nonparametric methods, parametric methods use rich prior information and perform superiorly. According to the adopted model, these methods can be divided into two subcategories. One of them is a fusion method based on the all-pole model proposed by Cuomo et al. [3] that builds linear models to predict signals. The model order is used to determine the number of poles, and the root-MUSIC and ordinary least squares methods are used to obtain pole estimates. Among them, only the poles closest to the unit circle are considered. The attenuation index and the relationship between the model order reduction method and the all-pole model show that these poles deviate from the unit circle in varying degrees due to the introduction of attenuation terms. Therefore, pole selection using root-MUSIC is not robust. Ideal results may be achieved when the signal-to-noise ratio (SNR) is very high. When the SNR is low, however, interference poles that originally deviate from the unit circle may be closer to the unit circle than the real poles, resulting in inaccurate pole

selection. Zou et al. proposed a matrix beam method to resolve the disadvantages of using root-MUSIC to determine the influence of noise on the poles, as well as a noise suppression method [4]. However, the fundamental disadvantage of the all-pole model cannot be remedied. For example, when the power function model has many points, the model approaches either infinity or zero at the end of the extrapolated data because the power is too large. Although the all-pole model can express the signal formula, the errors in the linear model cannot be fitted to the signal perfectly.

With the development of deep learning, it is being applied to radar high-resolution imaging. Orr et al. used deep neural network (DNN) to apply high-resolution radar to autonomous driving [5]. In modern battlefields, however, large bandwidth signals are often required. Niu et al. used DNN to combine synthetic aperture radar (SAR) images with electromagnetic (EM) reflection models to simulate target images at different imaging angles [6]. It is worth mentioning that there are limitations in obtaining real SAR images. Similarly, DNN is also widely used in the field of direction-of-arrival (DOA) estimation. Tang et al. combined DNN with the DOA estimation of millimeter-wave radar to achieve multitarget estimation [7]. Amrani et al. proposed a robust feature extraction method for SAR image target classification by adaptively fusing effective features from different CNN layers [8]. Amrani et al. proposed an efficient feature extraction and classification algorithm based on a visual saliency model [9]. Amrani and Jiang addressed the problem of SAR target classification by proposing a feature extraction method that takes advantage of exploiting the extracted deep features from CNNs on SAR images to introduce more powerful discriminative features and robust representation ability for them [10]. In addition, to follow the Nyquist sampling theorem, these methods often require a sampling frequency that is at least twice the bandwidth when sampling. Therefore, the use of DNN for large-bandwidth signal fusion of multi-subband signals will have a wide range of applications in modern battlefields.

Theoretically, the baseband signal can be obtained from the chirp echo signal after down-conversion and dechirp processing. Inverse discrete Fourier transform (IDFT) of the baseband signal is used to obtain the distance envelope of the target scattering point. DNN is suitable for high-resolution processing of target distance information, which can be obtained through the accumulated distance envelope information of each subband.

The principal contributions of this paper can be summarized as follows:

(1) We propose a multi-subband fusion algorithm based on DNN. In this study, the accumulation of the distance envelope of the multi-subband signal is input into the DNN, and the distance envelope of the synthesized broadband signal under high SNR is used as the label such that a high SNR range envelope of the synthesized wideband signal within the training range can be obtained

(2) Compared with the traditional all-pole model and noise suppression method, DNN avoids the power function error caused by the characteristics of the formula of the pole model and solves the inherent errors of linear model fitting nonlinear signals. Similarly, the inaccurate relationship between the pole and the unit circle caused by the root-MUSIC algorithm when the SNR is low is also resolved

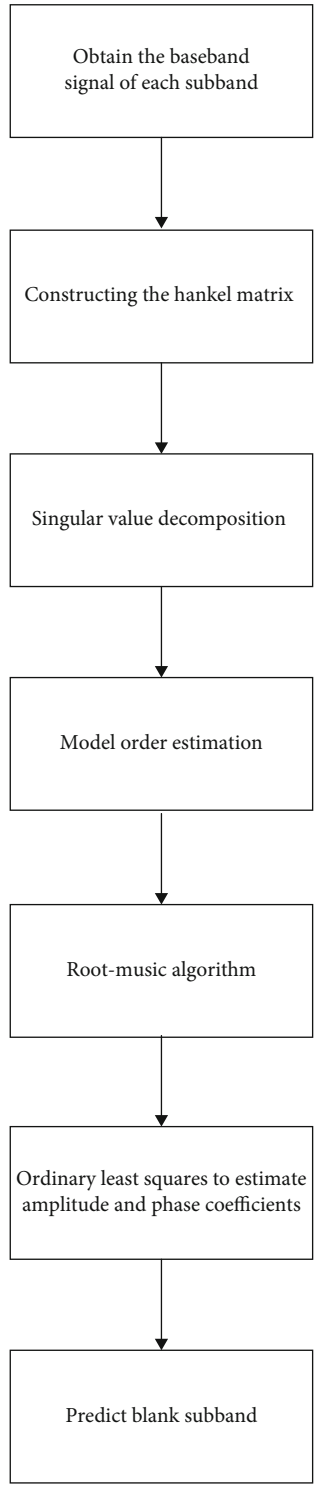

Figure 1: Flowchart of the all-pole model.

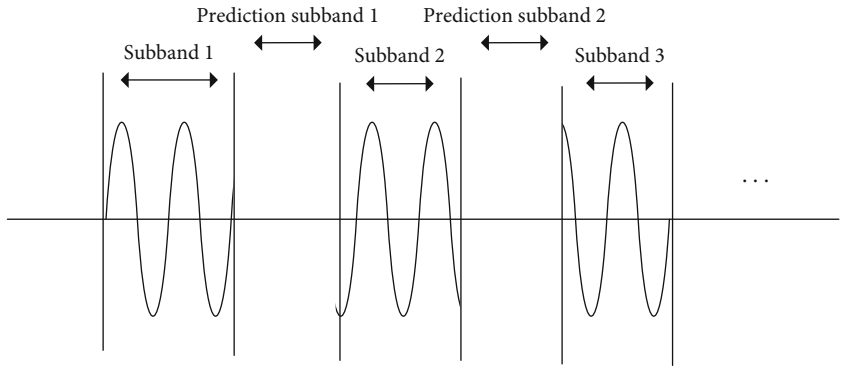

Figure 2: Schematic diagram of multi-subband signals.

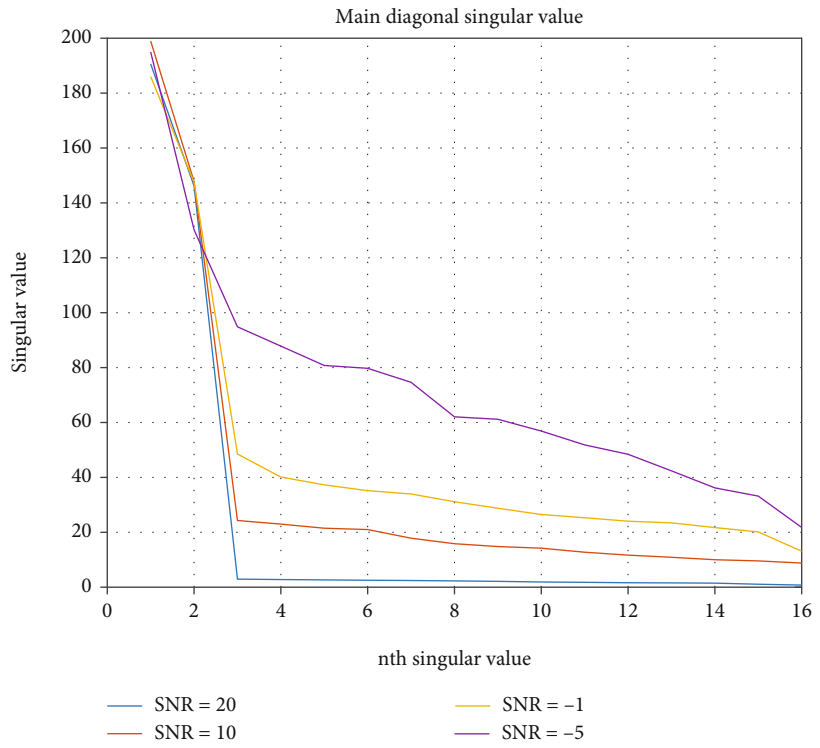

Figure 3: Singular value of main diagonal of the Hankel matrix before noise reduction.

The remainder of this paper is organized as follows: Section 2 describes the traditional signal fusion method, Section 3 describes the noise suppression method, Section 4 discusses the proposed algorithm and experimental results; and finally, Section 5 concludes the paper by summarizing the proposed work.

2. The Traditional Signal Fusion Method

Cuomo et al. proposed to use the pole information to coherently process and fuse the subbands with a linear model. Below is a flowchart to represent the all-pole model prediction algorithm (Figure 1).

Consider the following formula (1) where a chirp echo signal is used as an example.

$$s_0(t) = \sum_{i=1}^{m} A \exp\left\{ j2\pi \left[f_c(t-\tau_i) + \frac{K}{2}(t-\tau_i)^2 \right] \right\}. \quad (1)$$

Here, f_c represents the signal carrier frequency; m is the number of scattering points; t is time; K is the frequency modulation, which can be determined by the ratio of signal bandwidth, B, to time width, T_r; and τ_i is the delay of the i th scattering point, which is obtained by the ratio of twice the distance, R, to the speed of light, c.

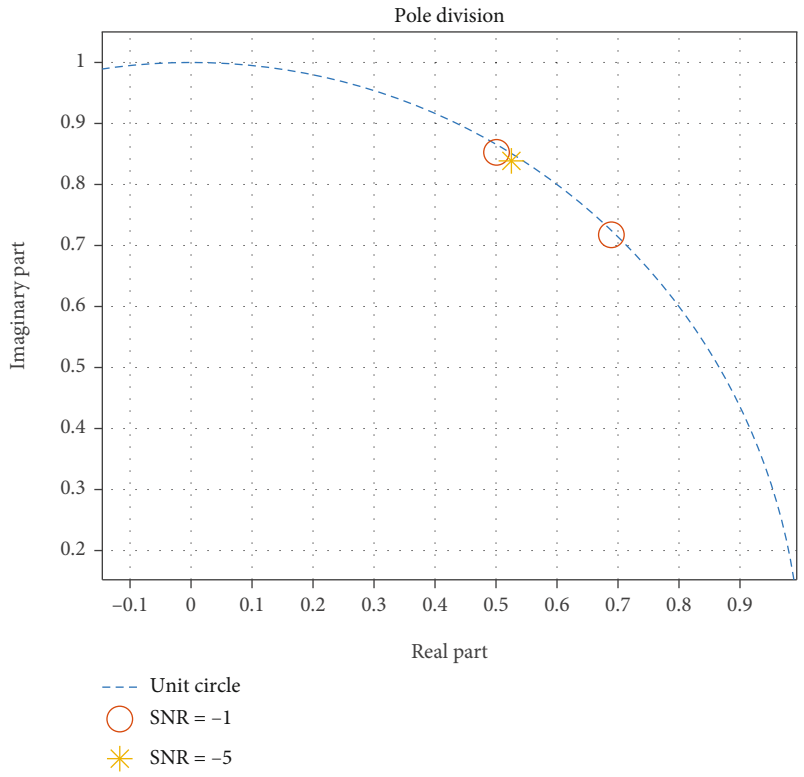

Figure 4: Pole distribution of subband 1 before noise suppression.

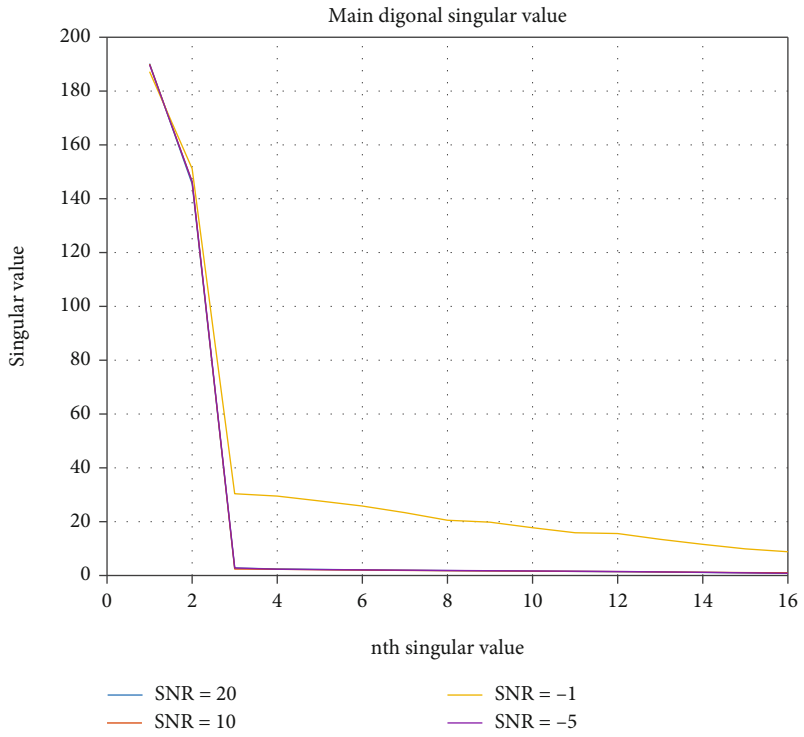

Figure 5: Singular value of main diagonal after noise suppression.

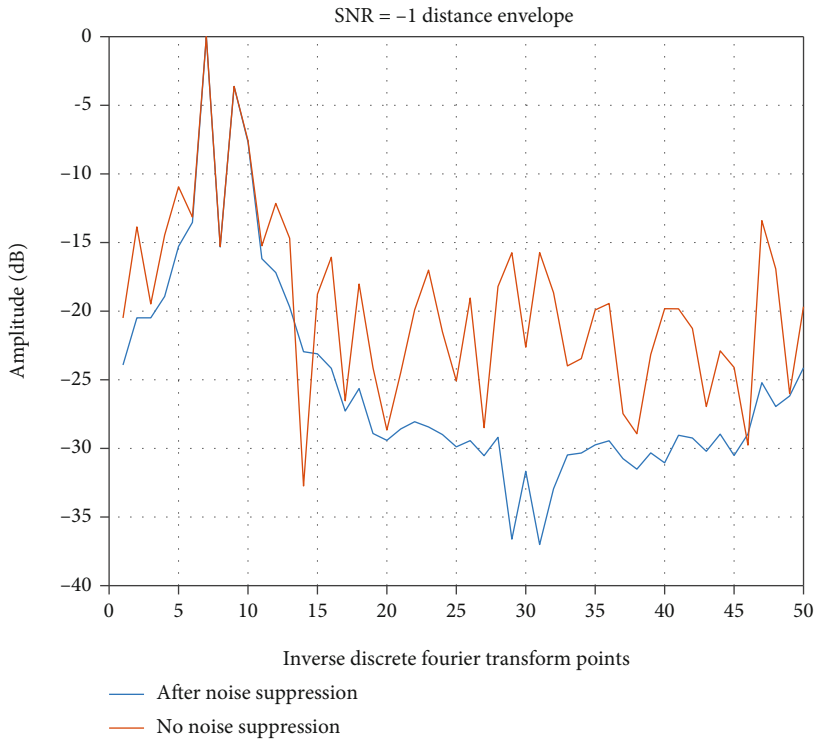

(a) SNR = −1 dB signal distance envelope after noise suppression

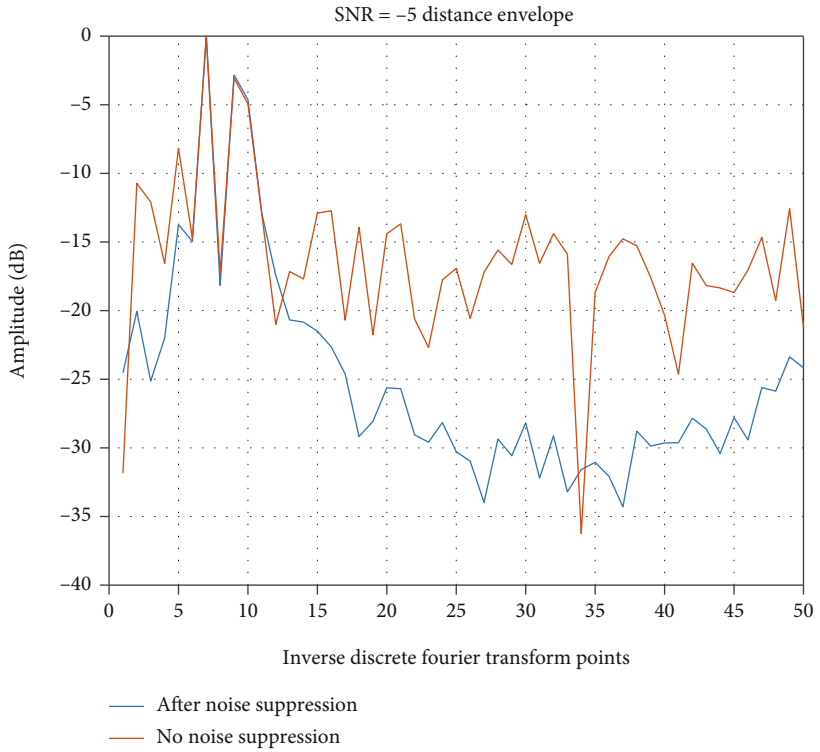

(b) SNR = −5 dB signal distance envelope after noise suppression

Figure 6: Signal distance envelope before and after noise suppression.

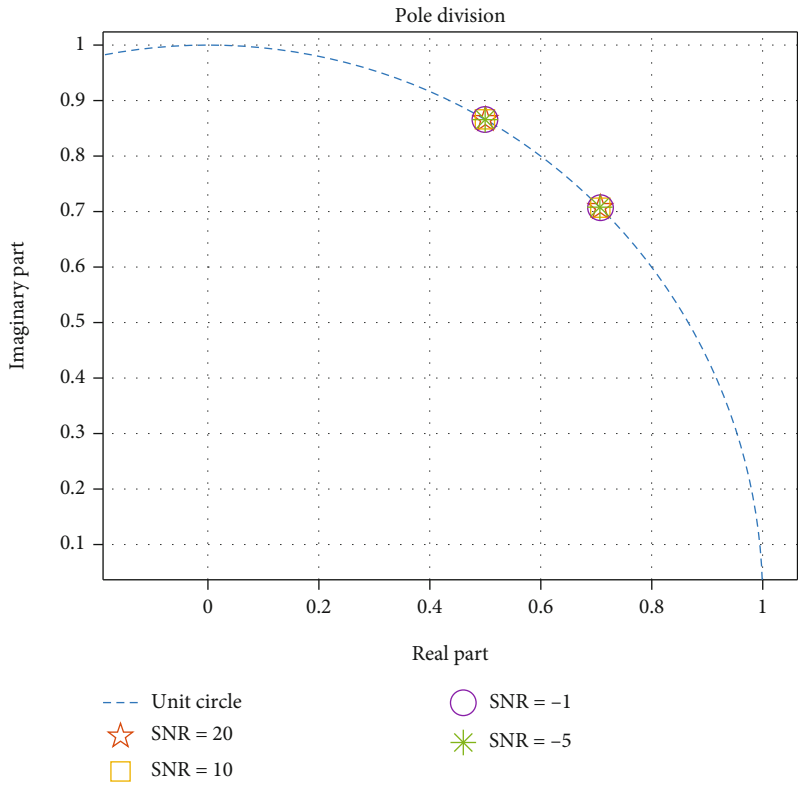

Figure 7: Pole distribution of subband 1 after noise suppression.

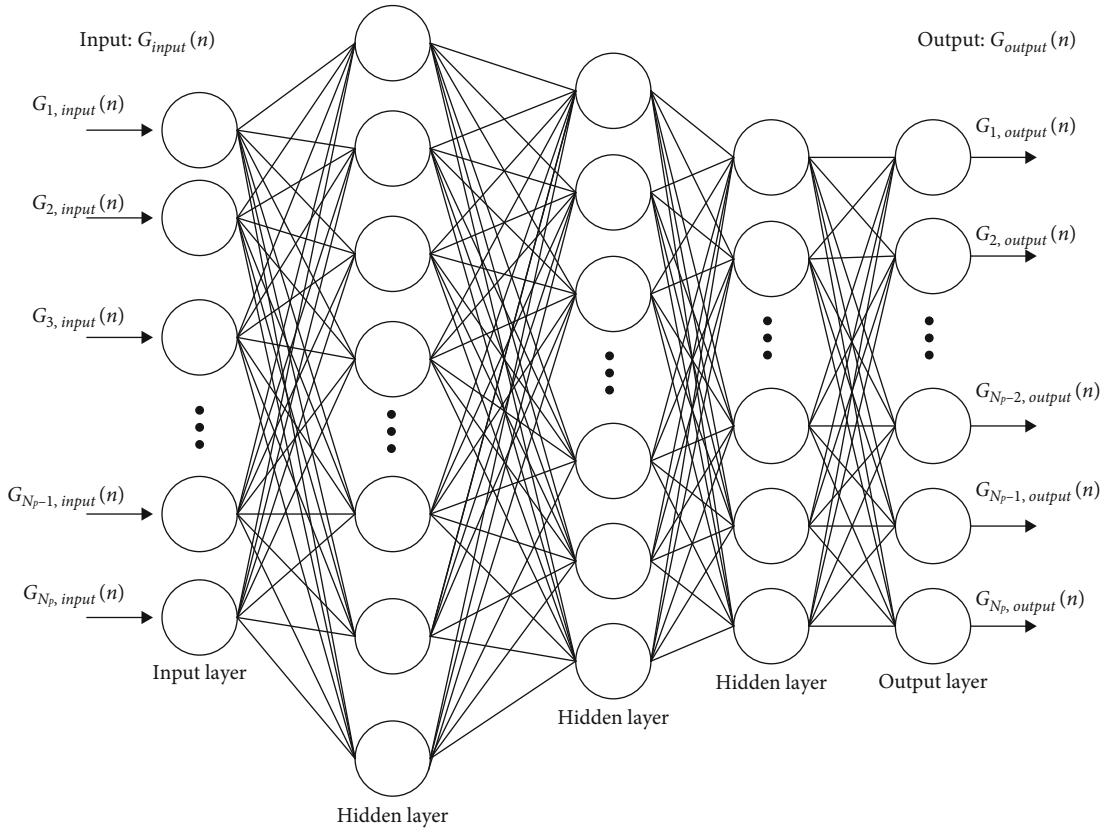

Figure 8: The DNN structure.

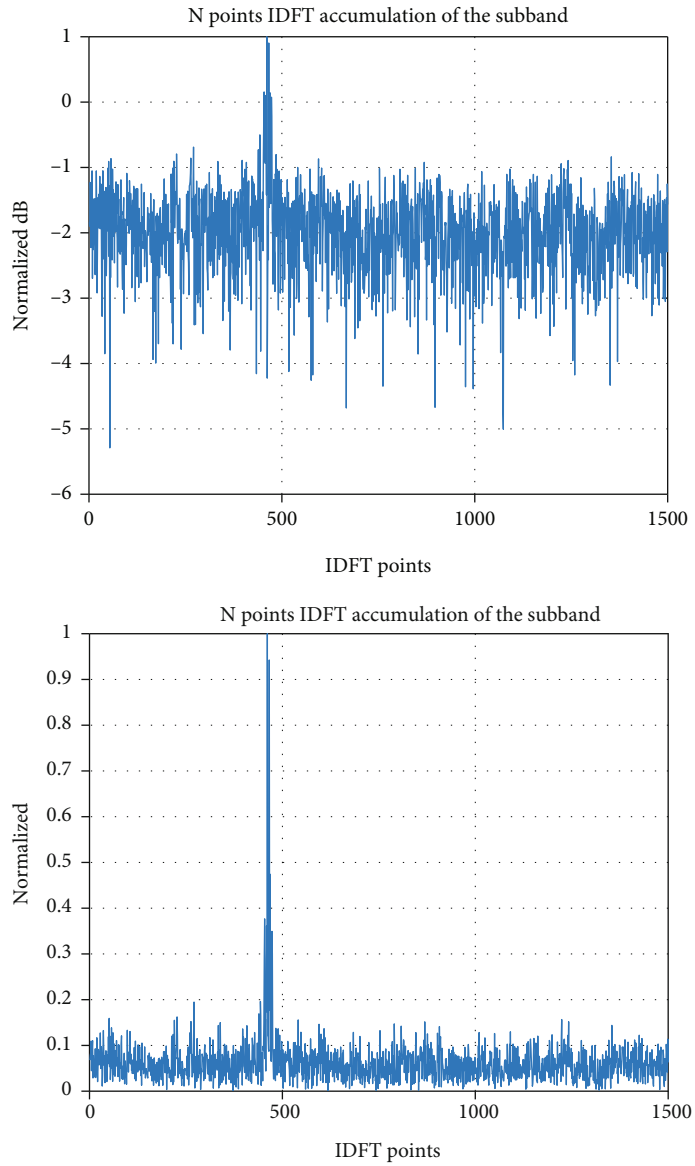

Figure 9: IDFT accumulation of N_p points of the subband.

The echo signal is multiplied by the basic frequency signal shown in formula (2) for defrequency modulation. This process is called down-conversion.

$$s_{f_c}(t) = \exp\left(-j2\pi f_c t\right). \tag{2}$$

The baseband signal of the radar echo signal can be defrequency-modulated by multiplying with formula (3) after down-conversion.

$$s_K(t) = \exp\left(-jK\pi t^2\right). \tag{3}$$

Thus, the baseband signal can be considered as the accumulation of single-frequency signals. The baseband signal can be expressed in the form shown in the following formula:

$$\begin{aligned} s(t) &= s_0(t) \cdot s_{f_c}(t) \cdot s_K(t) \\ &= \sum_{i=1}^{m} A \exp\left[j\pi\left(K\tau_i^2 - 2f_c\tau_i\right)\right] \cdot \exp\left(-j2\pi K\tau_i t\right) \\ &= \sum_{i=1}^{m} K_1 \cdot \exp\left(-j2\pi K\tau_i \frac{n}{f_s}\right), \\ s(n) &= \sum_{i=1}^{m} K_1 \cdot \left[\exp\left(-j2\pi\tau_i \frac{1}{f_s}\right)\right]^n, \\ K_1 &= A \exp\left[j\pi\left(K\tau_i^2 - 2f_c\tau_i\right)\right] \quad (n = 0, 1, \cdots, N-1). \end{aligned} \tag{4}$$

Here, N represents the number of baseband signal points, which can be obtained from the product of the sampling frequency, f_s, and the time width, T_r.

The all-pole model expresses the baseband signal as a linear model as shown in formula (5). Then, the vacant subband is predicted by calculating the pole point parameters.

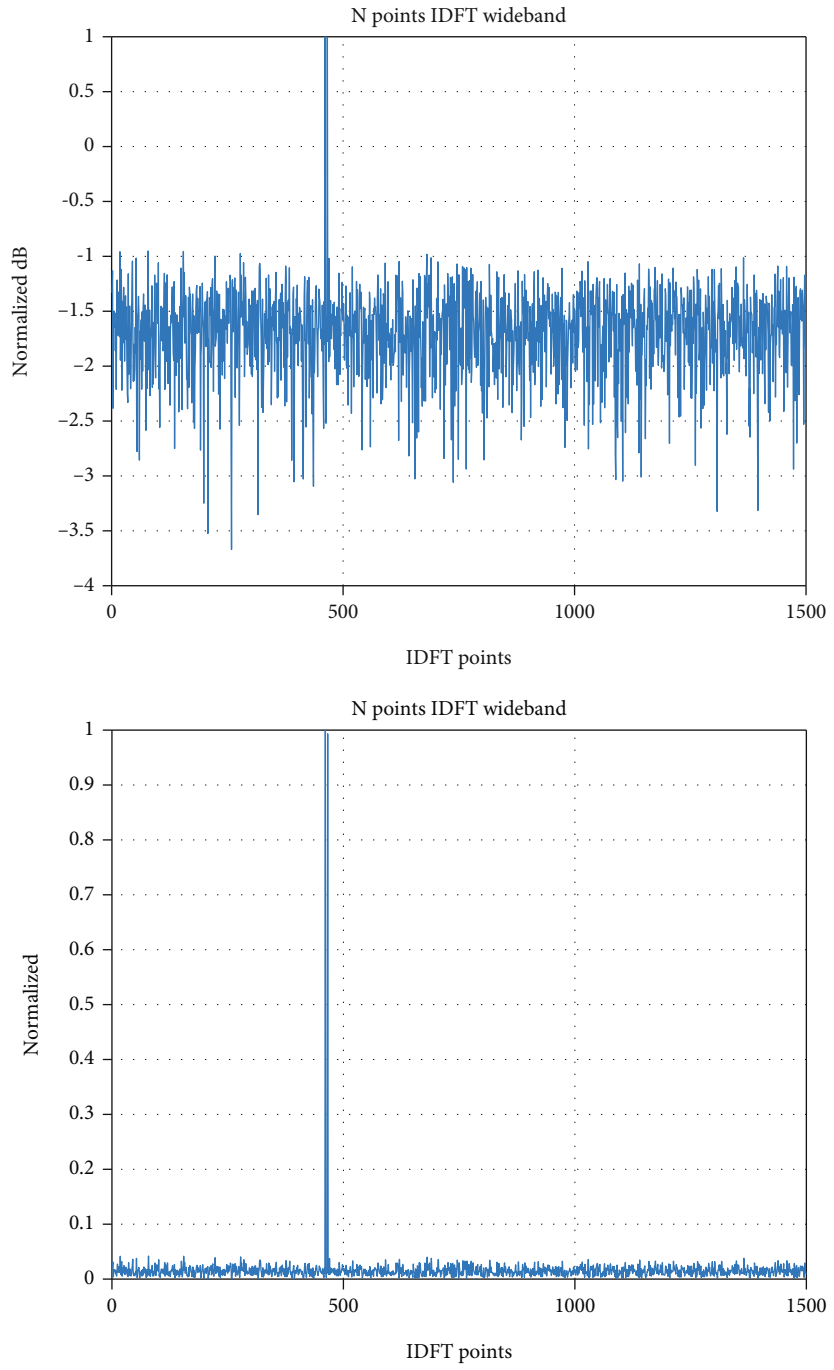

Figure 10: IDFT of N_p points of the wideband signal.

The schematic diagram of the multi-subband signal is shown in Figure 2.

$$M_k(n) = \sum_{k=1}^{P_k} a_k {p_k}^n, \quad n = 0, 1, \cdots, N-1,$$
$$a_k = A \exp\left[j\pi\left(K{\tau_i}^2 - 2f_c\tau_i\right)\right] = A \exp\left(j\varphi_k\right), \tag{5}$$
$$p_k = \exp\left(-j2\pi\tau_i \frac{1}{f_s}\right).$$

Here, $M_k(n)$ is the all-pole estimate; P_k is the number of poles, obtained according to Akaike information criterion (AIC) and the minimum description length (MDL), and also expressed as the number of scattering points; φ_k is the signal phase; a_k is the amplitude and phase coefficient of the poles; and p_k is the pole value of the model.

Regarding the three elements constructing a signal—amplitude, frequency, and phase—a_k represents the amplitude and phase coefficient of the signal, and p_k can solve for the frequency of a single-frequency signal.

The core of the algorithm is to construct a Hankel matrix for each subband after coherence. Then, the Hankel matrix is combined into a forward prediction matrix. Singular value decomposition is performed on the forward prediction matrix, from which the model order can be obtained from the main diagonal singular value. Subsequently, the pole value of the model is calculated according to the root-MUSIC algorithm. The pole point amplitude coefficient is then determined by substituting the pole point value into the least squares method. Finally, the vacant subband is estimated according to formula (5).

Multi-subband signal fusion is aimed at improving radar distance profiles. However, the model order of the traditional all-pole model algorithm needs to be determined according to the singular values of the main diagonal of the Hankel matrix constructed by the signal. When the SNR is low, the singular value curve gradually tends to be smooth as shown in Figure 3; this impacts the accuracy of the model.

The smoothing of the singular values of the main diagonal results in inaccurate determination of poles, as shown in Figure 4. The number of poles of a signal is different under low SNR, which has a great impact on the accuracy of the all-pole model.

Therefore, the traditional all-pole model has good performance in a high-SNR environment. However, it has too many shortcomings in its use in complex electromagnetic environments.

3. The Noise Suppression Method

A noise suppression method combining the singular values of the Hankel matrix is proposed in this section by processing the main diagonal values to suppress noise and improve the accuracy of the model.

Singular value decomposition is performed on the Hankel matrix, obtaining the following formula:

$$H = U * S * V^H. \tag{6}$$

Here, U and V are unitary matrices, V^H is the conjugate transpose of V, and S is the singular value matrix.

The main diagonal singular value is usually decreasing, and its value is expressed as a signal component. According to the model order, the smaller value represents the noise component, and the larger one represents the target component. The noise component can be set to a smaller value or zero to achieve noise suppression. As such, a new diagonal singular value S' is obtained. Then, the new Hankel matrix H' is reconstructed as in the following formula:

$$H' = U * \begin{bmatrix} S' & 0 \\ 0 & 0 \end{bmatrix} * V^H. \tag{7}$$

The reconstructed main diagonal singular values are shown in Figure 5. Compared with the main diagonal singular value without noise suppression, the singular value order is still obvious in low-SNR environments.

Table 1: Parameters of DNN.

Parameters	Values
Input dimension	1500
Output dimension	1500
Learning rate	0.000001
Optimization	AdamOptimizer
Epoch	15000
Activation function	ReLU
SNR	−20–0 dB
Initial distance	20–25 m
Relative distance	0.1–4 m
Scattering points	2–5
Number of train data	7920
Number of test data	2640

Formula (8) is used to reconstruct the signal after suppressing noise.

$$s'(t) = \frac{1}{m_n} \sum H'(i,j), \quad n = 1, 2, \cdots, N. \tag{8}$$

Here, m_n is the number of elements on the antidiagonal line in the matrix H', where the number of elements in $H'(i,j)$ meets $i + j - 1 = n$; and $\sum H'(i,j)$ represents the sum of the antidiagonal elements of the matrix H' each time.

IDFT was applied on the reconstructed signal to find the distance envelope, which has a higher SNR after noise suppression. Signals of SNR of −1 dB and −5 dB are shown in Figure 6 to illustrate and compare the results of their respective distance envelopes.

Determining the pole order from the Hankel matrix after noise suppression revealed that the pole values after noise suppression were accurate, as shown in Figure 7.

Although the algorithm can resolve the inaccuracies in pole distribution of the traditional method, it cannot compensate for the errors in the linear model in approximating the nonlinear signal. In addition, the traditional algorithm has many links; and the fusion of the vacant subband and the multi-subband predicted under various linear calculations still has a large root mean square error (RMSE) with the signal of the whole frequency band.

4. Using the DNN for Subband Fusion

In this section, we take the absolute value of the IDFT of the baseband signal to obtain the range profile of the target. A multi-subband distance envelope at low SNR is used as input, and the distance envelope of wideband signal is used as label to the network training under high SNR. The restriction of the traditional pole model at low SNR using the root-MUSIC algorithm may be improved via DNN nonlinear fitting. Thus, a more accurate range profile can be obtained compared with traditional subband fusion algorithms. The structure of the DNN is represented in Figure 8.

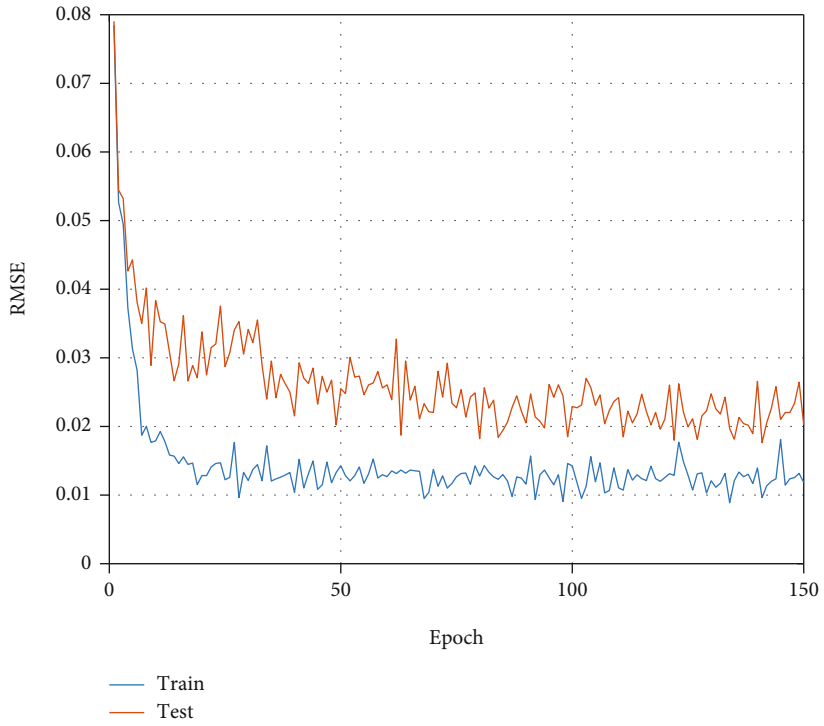

Figure 11: RMSE of training data set and test data set.

The network is divided into five layers, the input layer, three hidden layers, and an output layer. The activation function is the rectified linear unit (ReLU) function. The output of the l layer constitutes a vector a^l of $n \times 1$, expressed by the matrix in the following formula:

$$a_j^l = \sigma\left(z_j^l\right) = \sigma\left(\sum_{k=1}^{m} W_{jk}^l a_k^{l-1} + b_j^l\right). \tag{9}$$

The forward propagation algorithm is expressed as using several weight coefficient matrices, W, and the bias vector, b, to perform operations with the input value vector. Starting from the input layer, backward calculations are performed at each layer, up to the output layer, until the output layer where the result is obtained. The forward propagation algorithm of DNN is expressed by formula (10), the output of which then can be expressed as a^l.

$$a^l = \sigma\left(z^l\right) = \sigma\left(W^l a^{l-1} + b^l\right). \tag{10}$$

Before executing the DNN back propagation algorithm, a method to measure the loss between the output calculated by the training sample and the output of the real training sample is to be chosen. Herein, the common RMSE is used to measure the loss. For each sample, formula (11) is to be minimized.

$$\mathrm{RMSE} = \sqrt{\frac{1}{N}\sum_{i=1}^{n}\left(a^l - y\right)^2}. \tag{11}$$

Here, a^l and y are vectors whose feature dimension is the output layer. So, for the parameters of the output, the loss function becomes

$$\mathrm{RMSE}(W, b, x, y) = \sqrt{\frac{1}{N}\sum_{i=1}^{n}\left(\sigma\left(W^l a^{l-1} + b^l\right) - y\right)^2}. \tag{12}$$

Then, the gradients of W and b are expressed via formulas (13) and (14), respectively.

$$\frac{\partial \mathrm{RMSE}(W, b, x, y)}{\partial W^l} = \left[\left(a^l - y\right) \odot \sigma'\left(z^l\right)\right]\left(a^l - 1\right)^T, \tag{13}$$

$$\frac{\partial \mathrm{RMSE}(W, b, x, y)}{\partial b^l} = \left(a^l - y\right) \odot \sigma'\left(z^l\right). \tag{14}$$

The symbol $\odot$ here represents the Hadamard product. For two vectors, $A(a_1, a_2, \cdots a_3)^T$ and $B(b_1, b_2, \cdots b_3)^T$ with the same dimensions, $A \odot B = (a_1 b_1, a_2 b_2, \cdots a_n b_n)^T$.

When solving W and b of the output layer, the intermediate dependent part, $(\partial \mathrm{RMSE}(W, b, x, y))/\partial z^l$, is calculated using the following formula:

$$\delta^l = \frac{\partial \mathrm{RMSE}(W, b, x, y)}{\partial z^l} = \left(a^l - y\right) \odot \sigma'\left(z^l\right). \tag{15}$$

According to the forward propagation algorithm in formula (10), the gradients of W^l and b^l of the lth layer are easily calculated via formulas (16) and (17), respectively.

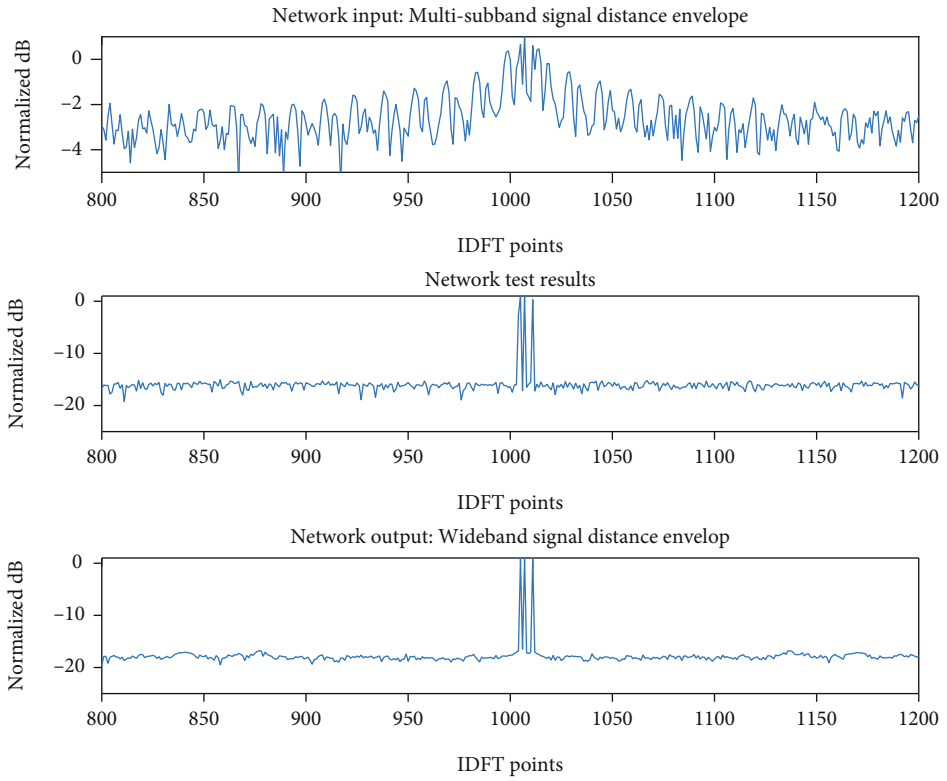

(a) SNR = −15 dB; initial distance = 23 m; scattering points = 3

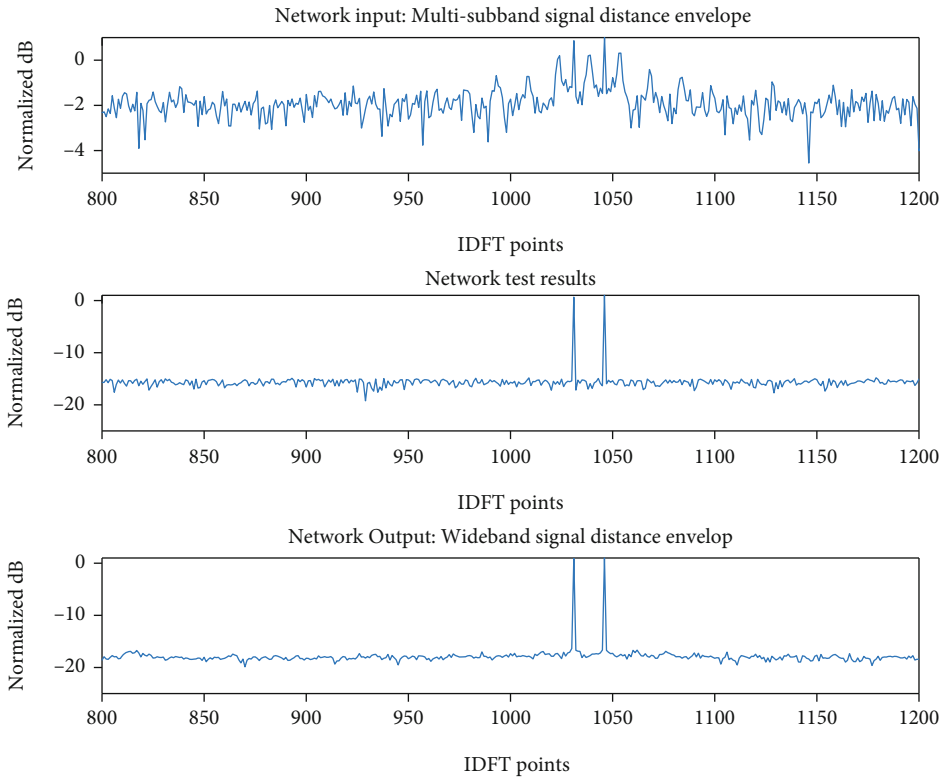

(b) SNR = −10 dB; initial distance = 25 m; scattering points = 2

Figure 12: Continued.

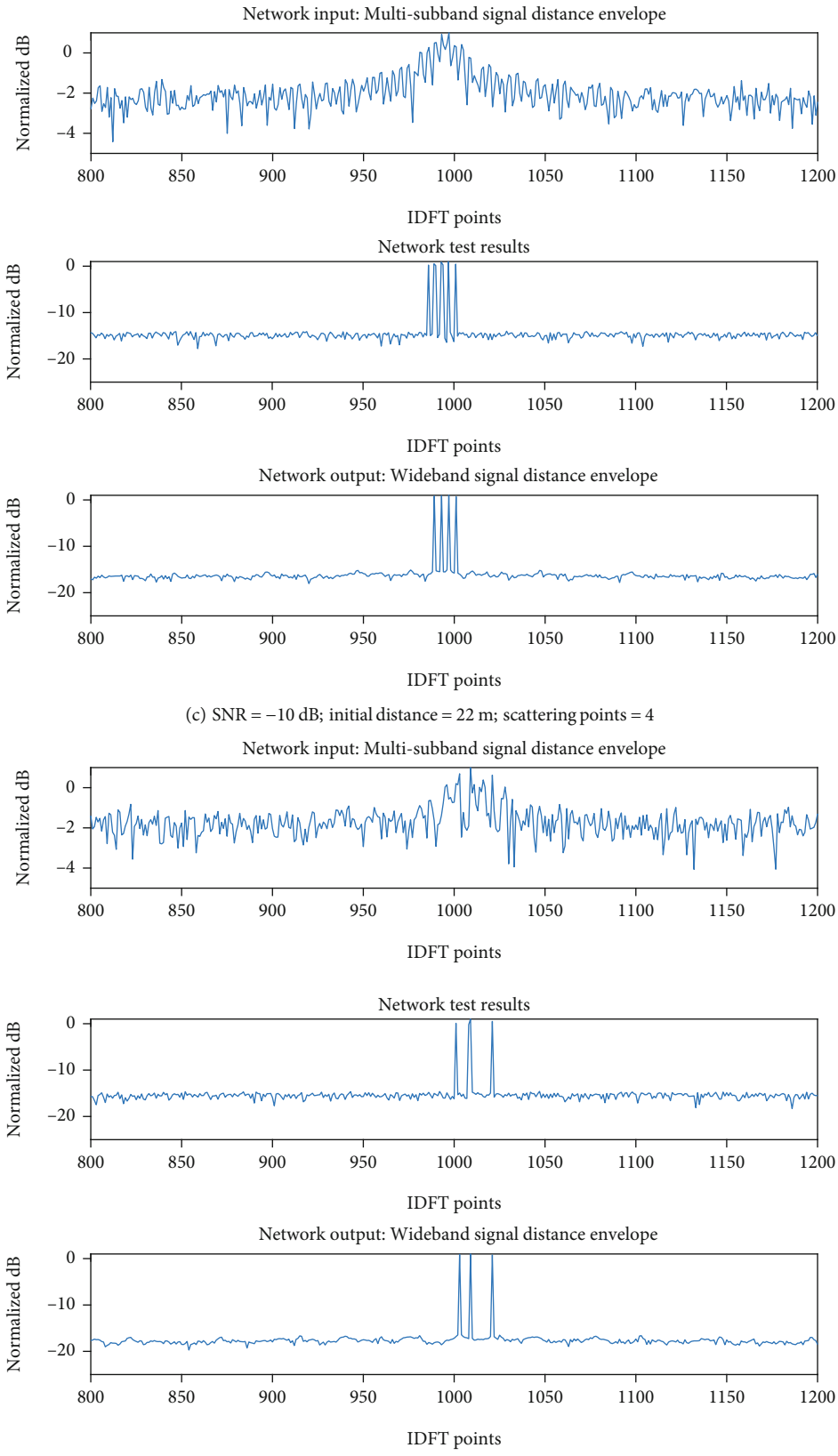

(c) SNR = −10 dB; initial distance = 22 m; scattering points = 4

(d) SNR = −10 dB; initial distance = 23 m; scattering points = 3

Figure 12: Continued.

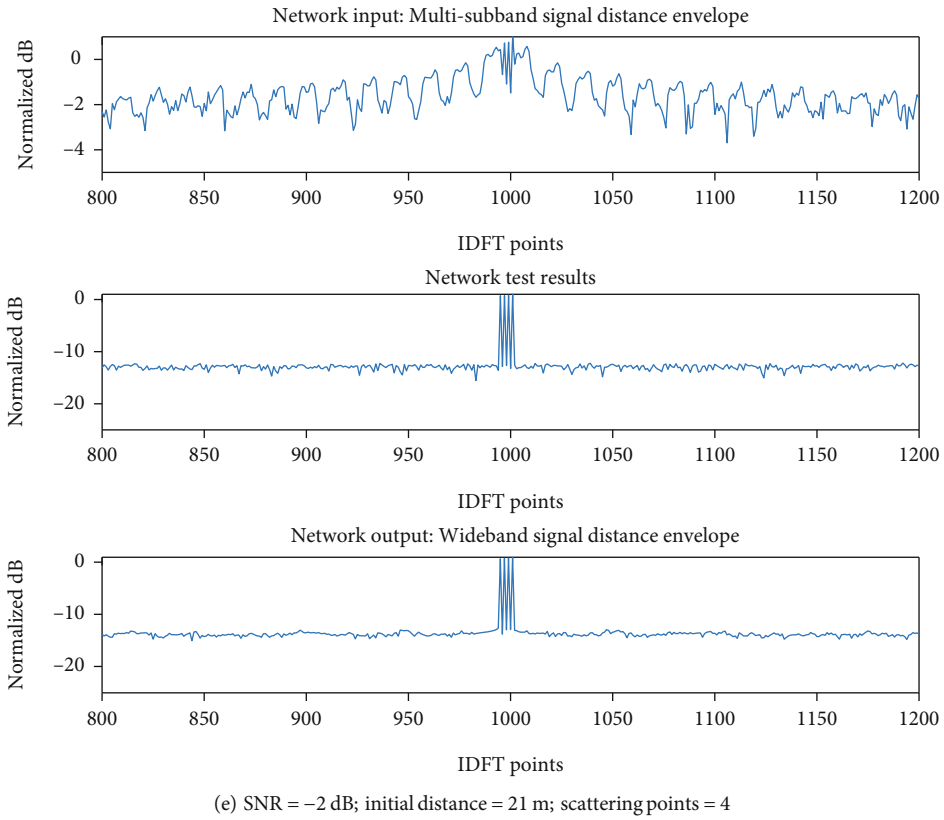

(e) SNR = −2 dB; initial distance = 21 m; scattering points = 4

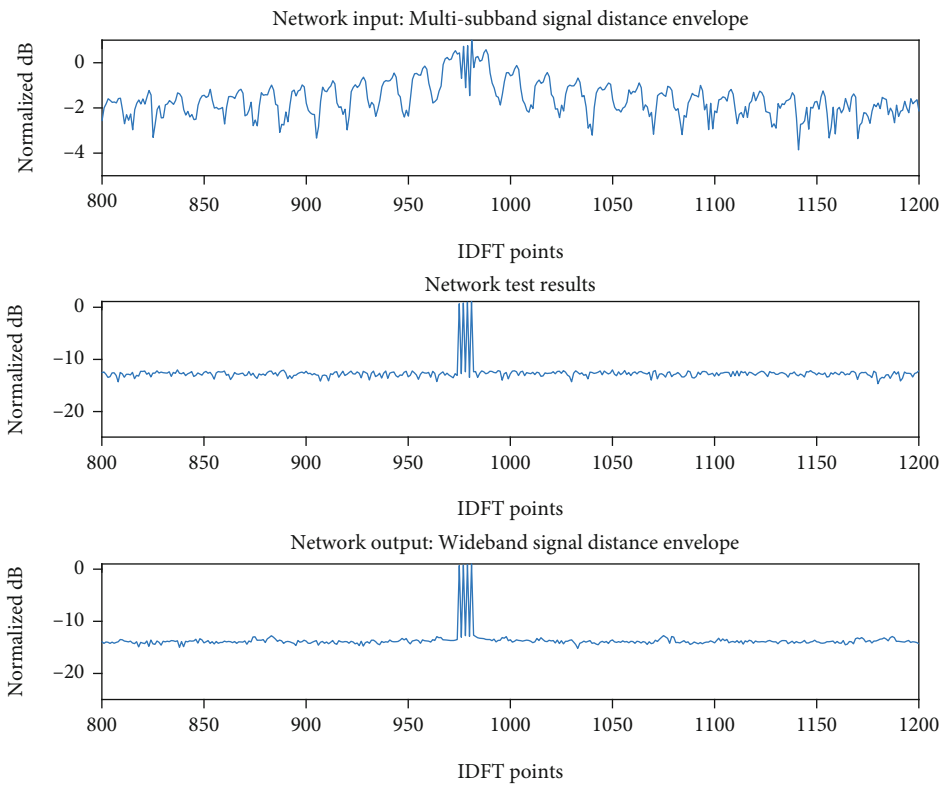

(f) SNR = −2 dB; initial distance = 20 m; scattering points = 5

Figure 12: Comparison of test results.

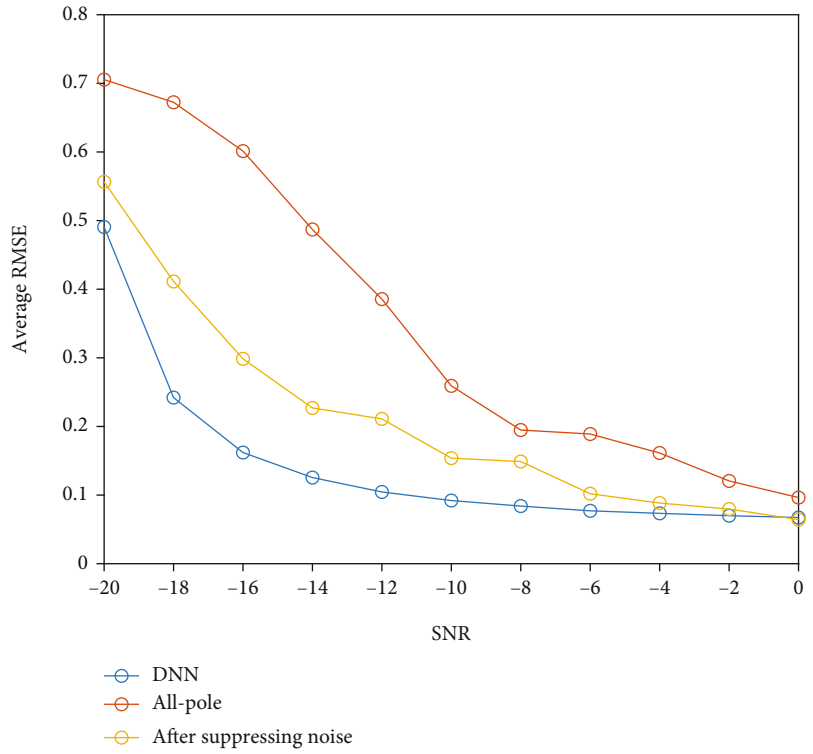

Figure 13: Comparison of the traditional algorithm, noise reduction algorithm, and DNN RMSE.

$$\frac{\partial \mathrm{RMSE}(W,b,x,y)}{\partial W^l} = \delta^l \left(a^l - 1\right)^T, \tag{16}$$

$$\frac{\partial \mathrm{RMSE}(W,b,x,y)}{\partial b^l} = \delta^l. \tag{17}$$

Through these formulas, the W^l and b^l of the lth layer may be continuously updated to complete the back propagation.

Now, the distance envelope of the baseband signal is obtained by the IDFT of formula (4), shown in the following formula:

$$G(k) = \left|\mathrm{IDFT}[s(n), N]\right| = \left|\frac{1}{N}\sum_{k=1}^{N}\sum_{i=1}^{m} K_1 \cdot \exp\left[j\frac{2\pi}{N}n(k - B\tau)\right]\right|. \tag{18}$$

Here, N is the number of points of IDFT.

When $k = B\tau$, the absolute value of $G(k)$ is at maximum. Therefore, the distance envelope of the baseband signal is only related to τ, which is the function related to R.

The input of the network is expressed in formula (19), and its label is expressed in formula (20).

$$G_{\mathrm{input}}(n) = \sum_{i=1}^{p}\left|\mathrm{IDFT}\left[s_{2i-1}(n), N_p\right]\right| + \sum_{i=1}^{p}\left|\mathrm{IDFT}\left[n_i(n), N_p\right]\right| \quad (n \in [1 + 2(i-1)N_0, (2i-1)N_0), \tag{19}$$

$$G_{\mathrm{label}}(n) = \left|\mathrm{IDFT}\left\{[s(n) + n(n)], N_p\right\}\right|. \tag{20}$$

Here, $\mathrm{IDFT}[s_{2i-1}(n), N_p]$ represents the IDFT for N_p points for each subband, N_p represents the number of points of the wideband signal, N_0 represents the number of points of the subband signal, and $n_i(n)$ is expressed as a noise sequence. The IDFT accumulation of N_p points of the subband and the wideband signal is illustrated in Figures 9 and 10, respectively.

Therefore, for the DNN, the relationship between the input and the label can be expressed by formula (21). Through the rules of forward propagation and back propagation, the RMSE value can be minimized continuously to minimize the error between the predicted result and the label between each layer.

$$G_{\mathrm{label}}(n) = \sum_{i}^{x} W_i G_{\mathrm{input}}(n) + b. \tag{21}$$

The SNR, the number of the scattering points, the initial distance between the scattering points and the radar, and the relative distance between the scattering points are all used as training set variables to generate the distance envelope training set. The data is generated by simulation, and the radar signals under different conditions are arranged into a matrix input network. The parameters of the DNN are shown in Table 1.

The DNN is used to calculate the input data and output data. After several iterations of training, the weights of each

neuron of the DNN model are adjusted by the error estimation results, and the training model is saved. In this study, RMSE is used to evaluate the performance of the network model. The RMSE is the average result of the test data. The above-mentioned mixed simulation data set was used for training. Figure 11 shows the change of RMSE with epoch. Via comparing the RMSEs of training and testing, consistency between the test and training data is achieved. The RMSE difference then is 0.01, which is considered as good performance for the DNN.

Comparing the test results of the subband distance envelope with the wideband signal distance envelope, the following conclusions were reached. First, the DNN has an accurate degree of fit for multiple scattered points, as shown in Figure 12. Second, the DNN can input the multi-subband distance envelope to directly obtain the wideband signal distance envelope. Third, training the DNN can omit the cumbersome steps that traditional algorithms need to estimate the signal. Fourth, a trained network can obtain more test results in batches, but the traditional algorithm must perform an overall calculation every time to obtain a test result. It is more advantageous to use the network when obtaining batch test data. More importantly, the RMSE of the results composed of complex data trained by the network is smaller than the RMSE of the single test data of the traditional algorithm. As shown in Figure 13, this also means that the network has higher accuracy than the traditional algorithms.

5. Conclusion

In this paper, an improvement to the traditional subband fusion algorithm and the use of DNN to obtain the distance envelope of the fused signal are proposed. Although noise suppression algorithms can improve the accuracy of traditional algorithms in low-SNR environments, they are yet unable to avoid the inherent errors of linear models. However, the use of neural networks to resolve the problem of subband fusion results in lower rates of error. Also, the distance envelope was directly used as the experimental object in this study to reduce the error caused while predicting the subband. Moreover, neural networks can obtain test data in batches, which is impossible with traditional algorithms. The results show that the range profile RMSE of the complex data obtained through the DNN is higher than the RMSE of the single data of the traditional algorithm; i.e., the DNN has higher accuracy.

Data Availability

The data that support the findings of this study are available from the author upon reasonable request.

Conflicts of Interest

The authors declare that they have no conflicts of interest.

Acknowledgments

This work was supported by the Equipment Development Key Fund (6140415010102), National Natural Science Foundation of China (62071137), and Fundamental Research Funds for the Central Universities (3072021CF0816).

References

[1] E. G. Larsson, P. Stoica, and L. Jian, "Amplitude spectrum estimation for two-dimensional gapped data," *IEEE Transactions on Signal Processing*, vol. 50, no. 6, pp. 1343–1354, 2002.

[2] J. Tian, J. Sun, G. Wang, Y. Wang, and W. Tan, "Multiband radar signal coherent fusion processing with IAA and apFFT," *IEEE Signal Processing Letters*, vol. 20, no. 5, pp. 463–466, 2013.

[3] K. M. Cuomo, J. E. Piou, and J. T. Mayhan, "Ultra-wideband coherent processing," *The Lincoln Laboratory Journal*, vol. 10, no. 2, pp. 203–222, 1997.

[4] Y.-q. Zou, X.-z. Gao, and X. Li, "Multiband radar signal high precision fusion imaging method based on matrix pencil algorithm," *Systems Engineering and Electronics*, vol. 38, no. 5, p. 1017, 2016.

[5] I. Orr, M. Cohen, and Z. J. N. M. I. Zalevsky, "High-resolution radar road segmentation using weakly supervised learning," *Nature Machine Intelligence*, vol. 3, pp. 239–246, 2021.

[6] S. Niu, X. Qiu, B. Lei, and K. Fu, "A SAR target image simulation method with DNN embedded to calculate electromagnetic reflection," *IEEE Journal of Selected Topics in Applied Earth Observations and Remote Sensing*, vol. 14, pp. 2593–2610, 2021.

[7] G. Tang, X. Gao, Z. Chen, Y. Zhang, H. Zhong, and M. Li, "Deep neural network based multiple targets DOA estimation for millimeter-wave radar," in *2019 IEEE smart world, Ubiquitous Intelligence & Computing, Advanced & Trusted Computing, Scalable Computing & Communications, Cloud & big Data Computing, internet of people and Smart City Innovations*, pp. 433–438, Leicester, UK, 2019.

[8] M. Amrani, A. Bey, and A. Amamra, "New SAR target recognition based on YOLO and very deep multi-canonical correlation analysis," *International Journal of Remote Sensing*, pp. 1–20, 2021.

[9] M. Amrani, F. Jiang, Y. Xu, S. Liu, and S. Zhang, "SAR-oriented visual saliency model and directed acyclic graph support vector metric based target classification," *IEEE Journal of Selected Topics in Applied Earth Observations & Remote Sensing*, vol. 11, pp. 3794–3810, 2018.

[10] M. Amrani and F. Jiang, "Deep feature extraction and combination for synthetic aperture radar target classification," *Journal of Applied Remote Sensing*, vol. 11, no. 4, p. 1, 2017.